PHILOSOPHICAL TRANSACTIONS OF THE ROYAL SOCIETY A

rsta.royalsocietypublishing.org

Research

**Cite this article:** Marenzana M *et al*. 2014 Synchrotron- and laboratory-based X-ray phase-contrast imaging for imaging mouse articular cartilage in the absence of radiopaque contrast agents. *Phil. Trans. R. Soc. A* **372**: 20130127.
http://dx.doi.org/10.1098/rsta.2013.0127

One contribution of 16 to a Discussion Meeting Issue 'Taking X-ray phase-contrast imaging into mainstream applications' and its satellite workshop 'Real and reciprocal space X-ray imaging'.

**Subject Areas:**
medical physics

**Keywords:**
coded-aperture X-ray phase-contrast imaging, analyser-based synchrotron X-ray phase-contrast imaging, mouse articular cartilage, osteoarthritis, contrast-enhanced microCT, phosphotungstic acid stain

**Author for correspondence:**
Massimo Marenzana
e-mail: m.marenzana@imperial.ac.uk

Royal Society Publishing

# Synchrotron- and laboratory-based X-ray phase-contrast imaging for imaging mouse articular cartilage in the absence of radiopaque contrast agents

Massimo Marenzana[1,2], Charlotte K. Hagen[3], Patricia Das Neves Borges[1], Marco Endrizzi[3], Magdalena B. Szafraniec[3], Tonia L. Vincent[2], Luigi Rigon[4], Fulvia Arfelli[4], Ralf-Hendrik Menk[5] and Alessandro Olivo[3]

[1]Department of Bioengineering, Imperial College, London SW7 2AZ, UK
[2]Kennedy Institute of Rheumatology, Nuffield Department of Orthopaedics, Rheumatology and Musculoskeletal Sciences, University of Oxford, Oxford OX3 7HE, UK
[3]Department of Medical Physics and Bioengineering, UCL, London WC1E 6BT, UK
[4]Dipartimento di Fisica dell'Università degli Studi di Trieste, Via Valerio 2, Trieste 34100, Italy
[5]Sincrotrone Trieste SCpA, Strada Statale, Basovizza, Trieste 34149, Italy

The mouse model of osteoarthritis (OA) has been recognized as the most promising research tool for the identification of new OA therapeutic targets. However, this model is currently limited by poor throughput, dependent on the extremely time-consuming histopathology assessment of the articular cartilage (AC). We have recently shown that AC in the rat tibia can be imaged both in air and in saline solution using a laboratory system based on coded-aperture X-ray phase-contrast imaging (CAXPCi). Here, we explore ways to extend the methodology for imaging the much thinner AC of the mouse, by means of gold-standard synchrotron-based phase-contrast methods. Specifically, we have

used analyser-based phase-contrast micro-computed tomography (micro-CT) for its high sensitivity to faint phase changes, coupled with a high-resolution (4.5 µm pixel) detector. Healthy, diseased (four weeks post induction of OA) and artificially damaged mouse AC was imaged at the Elettra synchrotron in Trieste, Italy, using the above method. For validation, we used conventional micro-CT combined with radiopaque soft-tissue staining and standard histomorphometry. We show that mouse cartilage can be visualized correctly by means of the synchrotron method. This suggests that: (i) further developments of the laboratory-based CAXPCi system, especially in terms of pushing the resolution limits, might have the potential to resolve mouse AC *ex vivo* and (ii) additional improvements may lead to a new generation of CAXPCi micro-CT scanners which could be used for *in vivo* longitudinal pre-clinical imaging of soft tissue at resolutions impossible to achieve by current MRI technology.

## 1. Introduction

Osteoarthritis (OA) is a pathology of the articular joint affecting up to one-third of the population older than 50 years and, owing to the current lack of effective treatments, its prevalence and social burden is predicted to increase with the ageing population worldwide [1]. This lack of progress in the development of effective cures for OA is largely due to the difficulty in diagnosing early cartilage lesions. The mouse model of OA is currently widely regarded as the most promising tool in OA research for its amenability to genetic modifications, which are crucial for the identification of new therapeutic targets and diagnostic biomarkers [2,3]. However, the potential of the mouse model of OA is currently limited by its poor throughput, largely dependent on the extremely time-consuming histopathology assessment of the articular cartilage (AC). Besides the time and costs involved, the histology-based approach is by definition destructive and prone to artefacts or losses owing to poor morphology and/or orientation. Moreover, conventional histology does not allow the sample structure to be reconstructed and visualized in three dimensions, and neither simultaneous, multiple views (e.g. coronal and sagittal and cross-sectional) of the sample nor three-dimension-based quantitative measurements such as tissue volume, thickness and surface are possible.

Therefore, non-invasive, high-throughput, quantitative techniques to evaluate murine AC are a major current need in OA research and are expected to greatly advance the field.

Recent progress in high-resolution micro-computed tomography (micro-CT) imaging combined with ionic partition equilibrium contrast agents, either cationic [4] or anionic [5], promises to provide useful functional information about pathological changes in the cartilage of small rodent models of OA. However, the structural information provided is often affected by the tissue composition (owing to differential binding of these contrast agents to healthy versus diseased cartilage). More crucially, these techniques are mostly limited to *ex vivo* applications owing to the variability of the uptake of different contrast agents *in vivo*.

Therefore, contrast agent-free, phase-based X-ray methods might offer an attractive solution. Such methods have been used on cartilage before, often on thicker human cartilage samples [6–8]. There is also an example of this approach *in vivo* on medium-sized laboratory rodents (guinea pig) which showed excellent results [9], but the main problem is that these studies typically require access to synchrotron facilities, which does not allow a widespread use of the technology in laboratories worldwide. Currently, a few research laboratories have attempted to translate crystal methods into use with laboratory sources. Muehlenman *et al.* [10] were able to visualize correctly human cartilage using a conventional X-ray tube and a set-up that included a double-silicon crystal monochromator and a silicon crystal analyser positioned between the imaged object and the detector. However, this requires the selection of only one narrowly defined X-ray wavelength, thus severely penalizing the flux available from a conventional source. Alternatively, grating interferometry has been used in combination with conventional laboratory sources to image bone

and cartilage [11]. Stutman *et al.* [12] also showed the possibility of imaging porcine cartilage in water; however, this was only possible on the third Talbot order. In grating interferometry, increasing the Talbot order (and hence the distance between phase and analyser grating) increases the method's sensitivity, but also the coherence requirements imposed on the radiation source.

Additional disadvantages of this approach are flux limitations caused by the necessity of using a 'source' grating, increased dose owing to the post-sample gratings (which are built on relatively thick silicon substrates) and highly demanding alignment requirements. A 'single grating' version also exists, in which images are then analysed by means of Fourier methods; however, this was reported to affect spatial resolution and possibly sensitivity [13]. Another option is provided by free-space propagation approaches, which however require the use of either synchrotron or microfocal X-ray sources [14], owing to the stringent demands this approach imposes in terms of spatial coherence. In this area, a promising study demonstrated that murine cartilage can be imaged in a mouse model of rheumatoid arthritis, achieving qualitative diagnostic information similar to conventional histology [15]. However, the necessity of using a microfocal source translates into very long acquisition times, owing to the low emitted flux.

A further alternative approach, derived from the 'edge illumination' concept developed at Elettra (the synchrotron facility in Trieste, Italy) in the late 1990s [16], was used to extract phase-contrast information for some of the data presented in this study; synchrotron- and laboratory-based implementations of this method are reviewed in [17]. It is based on subdividing the radiation beam in one or more individual 'beamlets', each one of which, instead of illuminating the full pixel area, hits only its edge. If only the edge of the pixel is illuminated by radiation, with the beam straddling sensitive and insensitive regions, then it is very easy for a photon refracted by the sample to 'change its status' from detected to undetected (if initially it hit the pixel, and is then deviated outside it by the interaction with the sample), and vice versa.

Typically, in a synchrotron set-up, the beam is vertically very narrow, and only one row of pixels is used, with the single 'laminar' beam hitting the top or bottom edge of this pixel row. The method, however, is easily adapted to a plurality of detector lines by means of masks. The first mask, placed immediately before the sample, creates a plurality of individual beams, spaced at the same pitch as the detector pixels. Because, unless very specialized detectors are used, an insensitive region is not available in a two-dimensional detector, this is created by means of a second mask placed in contact with the detector, with the pitch also matching that of the pixel. In this way, the 'edge illumination' condition described above is repeated for every single line of pixels in a two-dimension detector. This technique, termed coded-aperture X-ray phase-contrast imaging (CAXPCi) [18], was demonstrated to provide intense phase signals with fully polychromatic beams and an uncollimated, unapertured source size of up to 100 μm [19]. Because of the much simplified set-up compared with other methods, the method is easily scalable and leads to exposure time reductions [20].

We have recently shown that CAXPCi can be used to successfully visualize the AC in rat knee, and we have demonstrated that small artificial lesions applied with a surgical scalpel can also be detected when the tissue is imaged in water [21]. Importantly, we have been able to use automated image analysis to quantitatively assess cartilage thickness in the projection images obtained, owing to the high contrast achieved. However, our current laboratory set-up has a maximum spatial resolution of approximately 20 μm, which, while sufficient for the imaging of rat cartilage, is not sufficient to resolve the details of mouse AC.

We are therefore interested in expanding the method, especially in terms of resolution, to be able to effectively image thin mouse AC (30–100 μm thick). Prior to that, we wanted to explore the potential that X-ray phase-contrast imaging has to correctly visualize such thin cartilage layers. This would provide both confirmation of the feasibility and important indications for the requirements that future developments of the laboratory-based CAXPCi system should fulfil. For these purposes, we decided to use analyser-based [6–10] synchrotron phase-contrast micro-CT (synXPC in the following), which is based on the introduction of an analyser crystal between the sample and the detector. The narrow reflectivity curve of the crystal is used to analyse the faint deviations in the X-ray direction (refraction) resulting from phase variations in the sample.

This method was chosen because of its very high sensitivity to faint phase changes [22], and because of the strong similarities between its operating principles and those of CAXPCi: these were originally observed when the latter method was first introduced [16], and were formally demonstrated more recently [23]. For the validation of the correctness of the visualization of cartilage in two dimensions and three dimensions, we used conventional histomorphometry and contrast-enhanced micro-CT, respectively. By means of these methods, we were able to show that synXPC micro-CT was capable of imaging correctly intact, artificially damaged (dents) and diseased (from a mouse model of OA) AC on the mouse tibial epiphysis. These results give a preliminary indication that an extension of the laboratory-based CAXPCi method could enable cartilage studies in the mouse model of OA, should it be possible to achieve similar levels of resolution through the development of an upgraded system, with the ultimate goal of developing a method enabling unstained *in vivo* scanning of mouse cartilage.

## 2. Methods

### (a) Biological samples

Mice were maintained and studied in compliance with UK Home Office regulations. Tibiofemoral joints were explanted from healthy naive adult (12 weeks old) mice (C57BL/6), fixed in 10% buffered formalin for 24 h and then stored in 70% ethanol. OA was induced in three mice by destabilization of medial meniscus (DMM) surgery on the right knee, whereas the left leg was used as the non-operated contralateral (CTRL) following procedures reported previously [24]. Mice were sacrificed four weeks post-surgery. Before imaging, samples were rehydrated in saline solution for at least 2 h and the joint was carefully disarticulated to expose the articular surface of the tibia without adjacent soft tissues (e.g. menisci, ligaments and opposing femur surface).

### (b) Image acquisition

For the CAXPCi experiment, rat tibias were cut longitudinally in sections (1–3 mm thick) to achieve clearer two-dimensional image projections. When this experiment was performed, CAXPCi CT had not yet been developed, hence we opted for a solution which would represent the only approximation achievable with the available system. While we acknowledge this might not provide an exact correspondence with the image quality which would be provided by means of CAXPCi CT, we aimed at achieving some proof-of-concept, preliminary results which would demonstrate sufficient levels of sensitivity, thus encouraging further developments. The set-up of this CAXPCi has been described previously [21].

In the synXPC experiment, as mentioned above, the analyser-based imaging method was employed. This makes use of Bragg diffraction from a perfect crystal positioned between the sample and the detector. The crystal reflects the beam onto the detector with an intensity that depends on the angle with which the beam impinges on the crystal. By rocking the crystal, a reflectivity curve (the rocking curve) can thus be measured, its maximum occurring when the beam hits the crystal at the Bragg angle. For imaging, a certain reflectivity value is chosen, and the crystal is rocked to the corresponding position. Placing an object in the beam before the crystal causes the X-rays to be deviated from their path (refraction). The crystal functions as an analyser for these slight changes in direction. We used a double-bounce Si(1,1,1) crystal at 17 keV. For all samples, we acquired images at three different positions of the rocking curve, corresponding to reflectivity values of 50% at angles lower than the Bragg angle ('minus' side), 100% ('top', i.e. the Bragg angle) and 50% on the plus side. By processing these three images according to the algorithm described in [25], we can extract an image that is purely due to refraction, whereas a single image (taken on one of the reflectivity curve's positions) shows combined phase and absorption information. For tomography, we acquired 720 projections at 0.25° angular steps, thus covering 180° in total. We used a Photonic Science charge-coupled device (CCD) detector with a pixel of 4.5 μm, resulting in an effective resolution of approximately 9 μm. Horizontally (i.e. in the

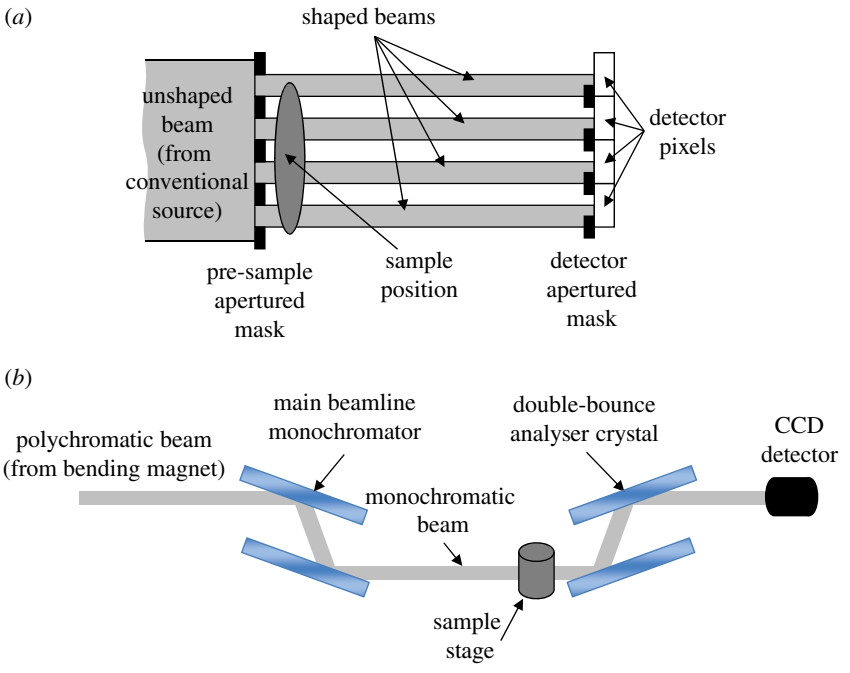


**Figure 1.** (*a*) Schematic of the laboratory-based CAXPCi set-up. (*b*) Schematic of the analyser-based phase-contrast imaging set-up used for the synchrotron experiment. (Online version in colour.)

direction orthogonal to the rotation axis), the full area was illuminated (4096 pixels corresponding to about 18 mm), whereas vertically the field of view is limited by the vertical dimensions of the synchrotron beam (3 mm).

From these images, three-dimensional volumes (either pure phase information or mixed phase and absorption) were reconstructed using the filtered-back projection algorithm [26]. The final (isotropic) voxel dimension was of 4.5 µm, although, as mentioned above, the effective resolution is approximately twice as much. Figure 1 shows a schematic representation of the CAXPCi and the synXPC set-ups.

## (c) Image analysis

A software procedure (Matlab platform; MathWorks, USA) was developed to analyse both CAXPC and synXPC images and perform an automated threshold-based measurement of cartilage thickness as previously described [21]. Briefly, after binarization, the top edge of the cartilage and its inner boundary (delimited by the mineralized cartilage) was identified using an edged detection algorithm. Briefly, a set of points corresponding to the first and second change from zero to 1 (i.e. from background to tissue) along the vertical axis of the image were classified. These points, which were distributed along either the upper or the lower edges of the cartilage, were then connected by interpolation with the best-fitting polynomial curves in order to compose the solid lines demarcating the edges of the mask enclosing the cartilage region. These masks were then validated by comparing them with the regions of interest (ROIs) obtained by manually contouring the cartilage layer and a strong agreement was found [21]. For the planar CAXPC images, the thickness of the AC was then calculated using a public domain plugin for ImageJ software, called BoneJ, which computes the average thickness of the ROI enclosing the cartilage as the average diameter of the best-fitting set of spheres [27]. For the synXPC micro-CT datasets and the contrast-enhanced micro-CT datasets, a volume of interest was determined by centring two rectangular ROIs on the central region of the two condyles of the tibia. The ROIs covered

a length of 800 μm (along the anterior–posterior axis, centred over the medial–lateral axis of the tibia) and had a width of 500 μm (along the medial–lateral axis, centred over the anterior–posterior midline of each tibial condyle). These regions coincide with the load-bearing regions in the tibial cartilage which are known to develop OA lesions in our mouse model. Moreover, as it is possible to computationally place these ROIs using the geometry and symmetry of each tibia, the computation of thickness and volume of the ROIs was performed automatically without the need for manual editing (which would have been otherwise required if the entire cartilage layer had been measured). For consistency, the cartilage thickness in the histological sections was measured in the same load-bearing regions with equally sized ROIs placed over each section (width of 500 μm).

### (d) Histomorphometry validation

Undecalcified samples were processed for methyl methacrylate embedding according to a previously described protocol [21]. Briefly, undecalcified samples were sectioned at a thickness of 8 μm, and sections were stained with toluidine blue, which reveals the hyaline as well as the calcified cartilage in a dark blue colour and the bone tissue in lighter blue. Some samples were also decalcified, embedded in paraffin and stained with a haematoxylin and eosin/safranin staining protocol as detailed previously [24]. Safranin stains hyaline and calcified cartilage in dark purple, whereas haematoxylin and eosin stain bone tissue in pink and cell nuclei in dark blue.

### (e) Contrast-enhanced micro-CT validation

Conventional micro-CT combined with a radiopaque stain for soft tissue was used as additional three-dimensional validation of the synXPC micro-CT images of the mouse AC.

The tibial epiphysis was incubated in a solution of 1% phosphotungstic acid (PTA) (a high-molecular-weight acid that binds preferentially to collagen) in 70% ethanol for 24 h as this procedure was previously shown to make the soft tissue of embryos stably radiopaque for conventional X-ray absorption micro-CT [28]. The tibiae were then scanned, within the same solution used for incubating the tissue, using a micro-CT scanner (1172 Skyscan, Belgium) with an isotropic voxel size of 5 μm (50 kV source voltage, 200 μA source current, 450 projection images, 590 ms exposure time for each projection image which was averaged four times, detector dimensions 2000 × 1048 pixels). The standard Feldkamp–Davis–Kress (FDK) reconstruction algorithm was used to generate cross-sectional images by means of the NRECON software package (SkyScan, Belgium). Images were compensated for misalignment, ring artefacts and beam hardening during reconstruction of images. To compensate for possible misalignments in the scan, the offset between the 0° and the 180° side projections was calculated automatically by NRECON software and an optimal overlay between the two projections was obtained prior to reconstruction. Ring artefacts, which may appear as a result of imperfections in the detector and cause concentric rings superimposed on the image, were minimized by randomly moving the object by a few micrometres throughout scanning [29] and by setting the ring artefact correction equal to 5 (as automatically set by the NRECON software) in the reconstruction process. To correct for beam hardening—which is a result of preferential absorption of low-energy X-rays on the surfaces of bone, leaving the inner portions apparently less dense owing to the fact that the remaining high-energy X-rays are absorbed less—the NRECON software applies mathematical corrections as documented in [30,31]. In this study, beam hardening was reduced both during the scans by using an aluminium filter and in the tomogram reconstruction by setting a constant beam hardening correction factor of 25% in the NRECON software.

## 3. Results

Figure 2*a* shows the strong refraction signal originated by the interface of the mouse AC visualized by high-resolution synXPC micro-CT (white arrowheads). The coronal image (resliced

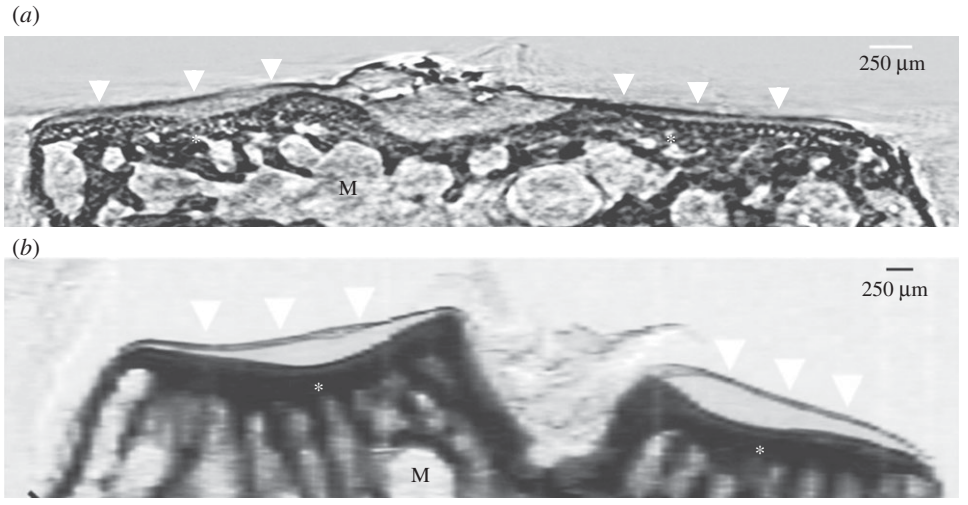


**Figure 2.** (*a*) A synXPC micro-CT image (4.5 µm thick virtual sections of the three-dimensional reconstruction) of the tibial epiphysis from a healthy naive adult mouse (C57BL/6, 12 weeks old) compared with (*b*) a CAXPC image (single two-dimensional projection) of a 1 mm thick coronal section of the tibial epiphysis imaged from a healthy naive adult rat (Sprague–Dawley, 12 weeks old). The surface of the articular cartilage is similarly clearly demarcated in both images (white arrowheads), whereas the deeper cartilage presents limited features (similar to the background). The bottom edge of the articular cartilage correctly, in both images, corresponds with the upper edge of the calcified cartilage (also known as the 'tidemark'). The subchondral bone features (asterisks) appear strongly contrasted over the bone marrow (M) background.

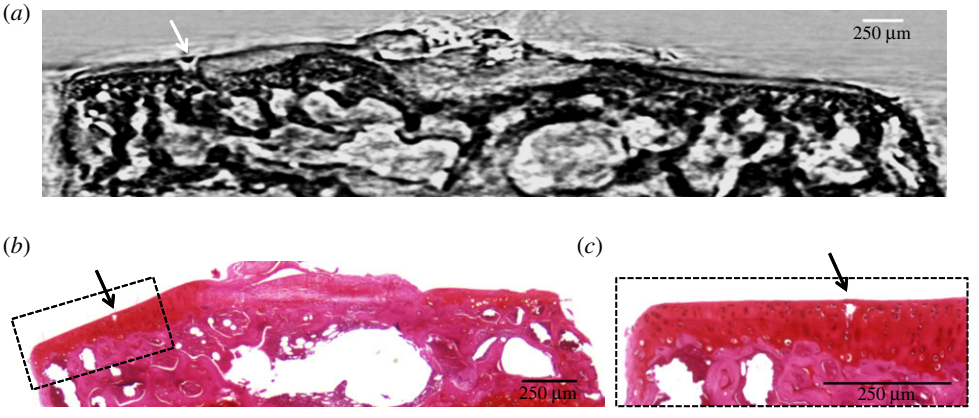


**Figure 3.** (*a*) A synXPC micro-CT coronal image of the same naive mouse tibial epiphysis shown in figure 1*a* but after applying an artificial lesion (white arrow) on the surface of the articular cartilage using a surgical scalpel; (*b*) histomorphometry validation of the synXPC image, showing the small lesion (black arrow) on the articular cartilage of the mouse tibial epiphysis (haematoxylin and eosin/safranin staining of decalcified paraffin sections); (*c*) close-up view of the portion of the cartilage with the lesion. (Online version in colour.)

from the three-dimensional reconstruction) of the mouse tibial epiphysis obtained by synXPC micro-CT enables the visualization of the cartilage interface in a (admittedly qualitatively) similar way to the image of the coronal section of rat tibial epiphysis obtained by CAXPCi (figure 2*b*). As can be seen, the cartilage in both images is clearly visualized, owing to a strong refraction signal coming from the interface. The bone trabecular structure left in the sample also seems correctly visualized, as is the growth plate cartilage. The two-dimensional morphological features were validated by histomorphometry (figures 3*b* and 4*c*). In order to assess the sensitivity of synXPC

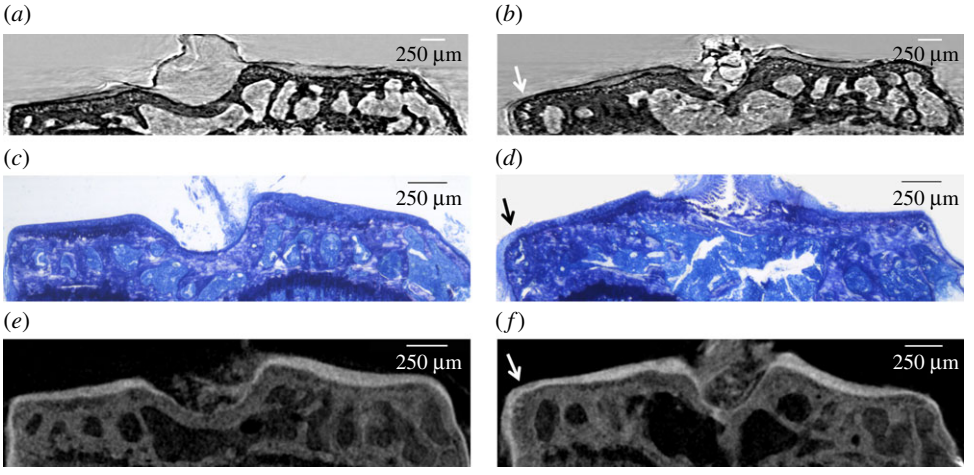


**Figure 4.** Coronal images of the tibial epiphysis from the surgical mouse model of osteoarthritis (at four weeks post-surgery), acquired by different imaging modalities. (*a*,*c*,*e*) Images of the contralateral (CTRL) non-operated tibia (left knee); (*b*,*d*,*f*) the DMM-operated tibia (right knee) of the same animal. (*a*,*b*) SynXPC micro-CT coronal images; (*c*,*d*) their respective histological validation (toluidine blue staining of undecalcified sections); (*e*,*f*) PTA contrast-enhanced micro-CT images as further validation. No evidence of cartilage lesions on the cartilage surface can be observed in any of images of the DMM-operated tibia (*b*,*d*,*f*). However, an osteophyte (arrow) growing at the medial margin of the joint and lined with a thick new layer of cartilage is clearly visible consistently in all three imaging modalities (*b*,*d*,*f*). (Online version in colour.)

micro-CT imaging to the detection of small cartilage lesions, a thin incision was then made by a surgical scalpel in the AC of the intact tibial epiphysis shown in figure 2*a* and then the sample was imaged again (figure 3*a*). The fissure-like lesion was very clearly visible in the synXPC image, and the presence of the lesion was confirmed by histomorphometry (figure 3*b*,*c*), at least within the constraints of being able to locate the same slice with two different techniques (it should also be noted that a small piece of tissue appears to have 'fallen over' the lesion, partially covering it near the cartilage surface, whereas a void remains underneath). We then imaged the tibiae obtained from mice that had OA induced in the right knee for four weeks by DMM surgery (figure 4). This early time point (four weeks post-surgery) for the severity of OA in the DMM model was chosen to determine the sensitivity of synXPC in detecting early OA features. The non-operated CTRL tibial epiphysis (figure 4*a*) appeared very similar to the healthy naive tibial epiphysis (figure 2*a*), and all features observed (e.g. intact AC layer, subchondral bone, marrow space) were validated by histomorphometry (figure 4*c*). Clear OA lesions were not found in the AC of the DMM sample (figure 4*b*), which is not surprising, given the early time point. The absence of superficial lesions on the AC of the DMM sample was confirmed by histopathology analysis (figure 4*d*). However, OA features, including a medial osteophyte and subchondral bone sclerosis, can be appreciated (figure 4*b*), and a reasonable confirmation of their presence is provided by the histological sections (figure 4*d*), notwithstanding the difficulties of isolating exactly the same slice in the two modalities. It is important to note the cartilage layer covering the medial osteophyte in the synXPC micro-CT images (figure 4*b* and validated in figure 4*d*), as this feature allows us to ascertain its osteophyte origin as opposed to a non-specific bone spur.

Finally, the same samples imaged by synXPC micro-CT were also incubated in PTA solution in order to stain the soft tissues for conventional X-ray absorption micro-CT imaging. This *ex vivo* stain protocol provided an excellent visualization of the AC, which was easily segmented automatically from the background and adjacent subchondral bone (figure 4*e*,*f*). Qualitatively, contrast-enhanced micro-CT images of the tibial epiphyses obtained from CTRL- and DMM-operated mice (figure 4*e*,*f*) appeared consistent with the synXPC images (figure 4*a*,*b*).

Quantitatively, automated three-dimensional image analysis showed that the AC average three-dimensional thickness (i.e. the thickness of the volume included in the load-bearing ROI on the medial side) was consistent between synXPC micro-CT (approx. 68 µm for CTRL and approx. 59 µm for DMM) and PTA contrast-enhanced micro-CT (approx. 65 µm for CTRL and approx. 55 µm for DMM, respectively). The average two-dimensional thickness of the AC (medial side) measured in histological sections was also consistent with the three-dimensional measurements (approx. 63 µm for CTRL and approx. 55 µm for DMM). Finally, the volume of AC (portion included in the load-bearing region) was measured in synXPC and gave the following values: for the CTRL AC, 0.033 $mm^3$ lateral side and 0.025 $mm^3$ medial side; for DMM AC, 0.033 $mm^3$ lateral side and 0.022 $mm^3$ medial side. Thus, both the thickness and volume of AC were found to be decreased in DMM compared with CTRL on the medial side but not on the lateral side of the tibia, indicating that synXPC imaging was sensitive to a reduction in AC thickness owing to OA (surgically induced on the medial side).

## 4. Conclusion

Our findings demonstrate that mouse AC can be visualized by high-resolution synXPC micro-CT, and that the image quality resembles that of rat cartilage imaged with the laboratory-based CAXPCi system, especially in terms of the mechanism that makes the cartilage layer visible (refraction). More detailed analysis over a wider range of samples will enable this similarity to be quantified and will help to define the requirements that a laboratory system should fulfil to enable the visualization of mouse AC, especially with regards to a CT extension which, as mentioned, was not available when this experiment was carried out but is now underway.

Our measurements of the mouse AC thickness imaged by synXPC micro-CT and PTA contrast-enhanced micro-CT were consistent and in line with other alternative three-dimensional methods (e.g. micro-CT with other contrast-enhancing stains or confocal microscopy) or histomorphometry measurements previously reported [32–34]. It is important to note that, different from most cited methods, both synXPC micro-CT and PTA contrast-enhanced micro-CT allowed a completely automated segmentation, owing to the high contrast achieved between the cartilage edges and the background or adjacent bone. One limitation of our study is that we used split joints (only the tibia) instead of the whole intact joints. However, the purpose of this paper was to provide evidence for the concept that CAXPCi can be potentially used to image mouse AC and therefore we focused on imaging hemi-joints where the exposed cartilage was the only relevant soft tissue. This approach also allowed us to develop automated image analysis (hence quantitative) to measure the geometry of the imaged AC (i.e. specifying automatically the edges of the AC and using standardized ROIs over the load-bearing regions of the tibial condyles).

PTA contrast-enhanced micro-CT provided a valuable three-dimensional reference (at comparable isotropic voxel resolution) to validate synXPC micro-CT images. To our knowledge, PTA has never been used before specifically as a contrast agent for imaging adult mouse AC by micro-CT, and this study shows that it is a very promising method for rapid *ex vivo* assessment of AC structures and lesions.

Our visualizations and quantitative results are also in full agreement with a recent paper which represents the most accurate imaging of mouse cartilage in three dimensions reported so far [35]. In this study, Ruan and co-workers used one of the most advanced commercial micro-CT scanners (which combines absorption and phase-contrast imaging modalities) and imaged mouse AC, pre-stained with osmium tetroxide mixed with ruthenium hexamine trichloride and cacodylic acid, at increasingly higher resolutions (10, 4, 2, 1.5 and 0.5 µm). Although highly accurate and informative, their approach required extremely long acquisition times (e.g. 17 h for the acquisition of approx. 2 µm resolution scans), which, combined with the use of toxic contrast agents, makes their method unsuitable for high-throughput assessments or *in vivo* imaging.

Our current proof-of-concept result is important because: (i) it gives promising indications on the potential for a higher resolution laboratory-based CAXPCi system to resolve mouse AC *ex vivo* in three dimensions without any contrast agents. The fact that the resolution in the synXPC

system was approximately twice that of the CAXPCi system would suggest that this could be within reach, although more detailed analysis (e.g. quantitative comparison between the signal-to-noise ratios obtained with the two systems) and tests are still required before firm conclusions can be drawn. (ii) In the longer term, further improvement in the CAXPCi system may lead to a new generation of CAXPCi micro-CT scanners, which could be used for *in vivo* longitudinal pre-clinical imaging of AC at resolutions impossible to achieve by current MRI technology. Notably, given the proven difficulties with contrast-enhanced micro-CT imaging of the mouse AC *in vivo*, X-ray phase-contrast micro-CT seems to provide the most valuable potential solution to bring the mouse model of OA to the next level in terms of throughput and translational applications. Some degree of promise in this sense is given by the fact that our preliminary studies on rat cartilage with the laboratory-based system were conducted at acceptable dose levels [21]; however, the main challenge will consist in being able to maintain comparable dose levels in the three-dimensional implementation of a system with at least twice the resolution.

Funding statement. This work was funded by the EPSRC (grants EP/G004250/1 and EP/I021884/1) and the Wellcome Trust/EPSRC Centre of Excellence for Medical Engineering Solutions in the Management of Osteoarthritis (grant no. 088844/Z/09/Z).

## References

1. Lawrence RC *et al*. 2008 Estimates of the prevalence of arthritis and other rheumatic conditions in the United States. Part II. *Arthritis Rheum.* **58**, 26–35. (doi:10.1002/art.23176)
2. Glasson SS. 2007 *In vivo* osteoarthritis target validation utilizing genetically-modified mice. *Curr. Drug Targets* **8**, 367–376. (doi:10.2174/138945007779940061)
3. Tremoleda JL, Khalil M, Gompels LL, Wylezinska-Arridge M, Vincent T, Gsell W. 2011 Imaging technologies for preclinical models of bone and joint disorders. *EJNMMI Res.* **1**, 11. (doi:10.1186/2191-219X-1-11)
4. Bansal PN, Joshi NS, Entezari V, Malone BC, Stewart RC, Snyder BD, Grinstaff MW. 2011 Cationic contrast agents improve quantification of glycosaminoglycan (GAG) content by contrast enhanced CT imaging of cartilage. *J. Orthop. Res.* **29**, 704–709. (doi:10.1002/jor.21312)
5. Xie L, Lin ASP, Guldberg RE, Levenston ME. 2010 Nondestructive assessment of sGAG content and distribution in normal and degraded rat articular cartilage via EPIC-microCT. *Osteoarthritis Cartilage* **18**, 65–72. (doi:10.1016/j.joca.2009.07.014)
6. Mollenhauer J *et al*. 2002 Diffraction-enhanced X-ray imaging of articular cartilage. *Osteoarthritis Cartilage* **10**, 163–171. (doi:10.1053/joca.2001.0496)
7. Muehleman C *et al*. 2004 X-ray detection of structural orientation in human articular cartilage. *Osteoarthritis Cartilage* **12**, 97–105. (doi:10.1016/j.joca.2003.10.001)
8. Coan P *et al*. 2010 Characterization of osteoarthritic and normal human patella cartilage by computed tomography X-ray phase-contrast imaging: a feasibility study. *Invest. Radiol.* **45**, 437–444. (doi:10.1097/RLI.0b013e3181e193bd)
9. Coan P, Wagner A, Bravin A, Diemoz PC, Keyriläinen J, Mollenhauer J. 2010 *In vivo* X-ray phase contrast analyzer-based imaging for longitudinal osteoarthritis studies in guinea pigs. *Phys. Med. Biol.* **55**, 7649–7662. (doi:10.1088/0031-9155/55/24/017)
10. Muehleman C, Li J, Connor D, Parham C, Pisano E, Zhong Z. 2009 Diffraction-enhanced imaging of musculoskeletal tissues using a conventional x-ray tube. *Acad. Radiol.* **16**, 918–923. (doi:10.1016/j.acra.2009.04.006)
11. Kido K, Makifuchi C, Kiyohara J, Itou T, Honda C, Momose A. 2010 Bone cartilage imaging with x-ray interferometry using a practical x-ray tube. *Proc. SPIE* **7622**, 76224O. (doi:10.1117/12.843655)
12. Stutman D, Beck TJ, Carrino JA, Bingham CO. 2011 Talbot phase-contrast x-ray imaging for the small joints of the hand. *Phys. Med. Biol.* **56**, 5697–5720. (doi:10.1088/0031-9155/56/17/015)
13. Bennett EE, Kopace R, Stein AF, Wen H. 2010 A grating-based single-shot x-ray phase contrast and diffraction method for *in vivo* imaging. *Med. Phys.* **37**, 6047–6054. (doi:10.1118/1.3501311)
14. Gundogdu O, Nirgianaki E, Che Ismail E, Jenneson PM, Bradley DA. 2007 Benchtop phase-contrast X-ray imaging. *Appl. Radiat. Isot.* **65**, 1337–1344. (doi:10.1016/j.apradiso.2007.07.009)

15. Lee YS *et al*. 2010 Articular cartilage imaging by the use of phase-contrast tomography in a collagen-induced arthritis mouse model. *Acad. Radiol.* **17**, 244–250. (doi:10.1016/j.acra.2009.09.015)
16. Olivo A *et al*. 2001 An innovative digital imaging set-up allowing a low-dose approach to phase contrast applications in the medical field. *Med. Phys.* **28**, 1610–1619. (doi:10.1118/1.1388219)
17. Endrizzi M *et al*. 2013 Edge illumination and coded-aperture X-ray phase-contrast imaging: increased sensitivity at synchrotrons and lab-based translations into medicine, biology and materials science. *Proc. SPIE* **8668**, 866812. (doi:10.1117/12.2007893)
18. Olivo A, Speller R. 2007 A coded-aperture technique allowing x-ray phase contrast imaging with conventional sources. *Appl. Phys. Lett.* **91**, 074106. (doi:10.1063/1.2772193)
19. Olivo A, Speller R. 2007 Modelling of a novel x-ray phase contrast imaging technique based on coded apertures. *Phys. Med. Biol.* **52**, 6555–6573. (doi:10.1088/0031-9155/52/22/001)
20. Olivo A, Ignatyev K, Munro PRT, Speller RD. 2011 Noninterferometric phase-contrast images obtained with incoherent x-ray sources. *Appl. Opt.* **50**, 1765–1769. (doi:10.1364/AO.50.001765)
21. Marenzana M, Hagen CK, Borges PDN, Endrizzi M, Szafraniec MB, Ignatyev K, Olivo A. 2012 Visualization of small lesions in rat cartilage by means of laboratory-based x-ray phase contrast imaging. *Phys. Med. Biol.* **57**, 8173–8184. (doi:10.1088/0031-9155/57/24/8173)
22. Diemoz PC, Bravin A, Langer M, Coan P. 2012 Analytical and experimental determination of signal-to-noise ratio and figure of merit in three phase-contrast imaging techniques. *Opt. Exp.* **20**, 27 670–27 690. (doi:10.1364/OE.20.027670)
23. Munro PRT, Hagen CK, Szafraniec MB, Olivo A. 2013 A simplified approach to quantitative coded aperture x-ray phase imaging. *Opt. Exp.* **21**, 11 187–11 201. (doi:10.1364/OE.21.011187)
24. Burleigh A, Chanalaris A, Gardiner M, Driscoll C, Boruc O, Saklatvala J, Vincent TL. 2012 Joint immobilisation prevents murine osteoarthritis, and reveals the highly mechanosensitive nature of protease expression *in vivo*. *Arthritis Rheum.* **64**, 2278–2288. (doi:10.1002/art.34420)
25. Rigon L, Arfelli F, Menk R-H. 2007 Generalized diffraction enhanced imaging to retrieve absorption, refraction and scattering effects. *J. Phys. Appl. Phys.* **40**, 3077. (doi:10.1088/0022-3727/40/10/011)
26. Diemoz PC, Bravin A, Glaser C, Coan P. 2010 Comparison of analyzer-based imaging computed tomography extraction algorithms and application to bone-cartilage imaging. *Phys. Med. Biol.* **55**, 7663–7679. (doi:10.1088/0031-9155/55/24/018)
27. Doube M, Kşosowski MM, Arganda-Carreras I, Cordelières FP, Dougherty RP, Jackson JS, Schmid B, Hutchinson JR, Shefelbine SJ. 2010 BoneJ: free and extensible bone image analysis in ImageJ. *Bone* **47**, 1076–1079. (doi:10.1016/j.bone.2010.08.023)
28. Metscher BD. 2009 MicroCT for comparative morphology: simple staining methods allow high-contrast 3D imaging of diverse non-mineralized animal tissues. *BMC Physiol.* **9**, 11. (doi:10.1186/1472-6793-9-11)
29. Raven C. 1998 Numerical removal of ring artefacts in microtomography. *Rev. Sci. Instrum.* **69**, 2978–2985. (doi:10.1063/1.1149043)
30. Brooks RA, Di Chiro G. 1976 Beam hardening in x-ray reconstructive tomography. *Phys. Med. Biol.* **21**, 390–398. (doi:10.1088/0031-9155/21/3/004)
31. Postnov AA, Vinogradov AV, Van Dyck D, Saveliev SV, De Clerck NM. 2003 Quantitative analysis of bone mineral content by x-ray microtomography. *Physiol. Meas.* **24**, 165–178. (doi:10.1088/0967-3334/24/1/312)
32. Kotwal N, Li J, Sandy J, Plaas A, Sumner DR. 2012 Initial application of EPIC-μCT to assess mouse articular cartilage morphology and composition: effects of aging and treadmill running. *Osteoarthritis Cartilage* **20**, 887–895. (doi:10.1016/j.joca.2012.04.012)
33. Moodie JP, Stok KS, Müller R, Vincent TL, Shefelbine SJ. 2011 Multimodal imaging demonstrates concomitant changes in bone and cartilage after destabilisation of the medial meniscus and increased joint laxity. *Osteoarthritis Cartilage* **19**, 163–170. (doi:10.1016/j.joca.2010.11.006)
34. Eltawil NM, De Bari C, Achan P, Pitzalis C, Dell'accio F. 2009 A novel *in vivo* murine model of cartilage regeneration. Age and strain-dependent outcome after joint surface injury. *Osteoarthritis Cartilage* **17**, 695–704. (doi:10.1016/j.joca.2008.11.003)
35. Ruan MZC, Dawson B, Jiang M-M, Gannon F, Heggeness M, Lee BHL. 2013 Quantitative imaging of murine osteoarthritic cartilage by phase-contrast micro-computed tomography. *Arthritis Rheum.* **65**, 388–396. (doi:10.1002/art.37766)